Ceramics International 48 (2022) 32064–32072

Contents lists available at ScienceDirect

Ceramics International

journal homepage: www.elsevier.com/locate/ceramint

Design of super-hard high-entropy ceramics coatings via machine learning

Xiaoqian Xu [a,b], Xiaobo Wang [c], Shaoyu Wu [a,b], Luchun Yan [b], Tao Guo [a,b,**], Kewei Gao [a,b], Xiaolu Pang [a,b,*], Alex A. Volinsky [d]

[a] Beijing Advanced Innovation Center for Materials Genome Engineering, University of Science and Technology Beijing, Beijing, 100083, China
[b] School of Materials Science and Engineering, University of Science and Technology Beijing, Beijing, 100083, China
[c] China United Gas Turbine Technology Co., Ltd., Beijing, 100015, China
[d] Department of Mechanical Engineering, University of South Florida, Tampa, FL, 33620, USA

ARTICLE INFO

Keywords:
High-entropy ceramic coatings
Machine learning
High-throughput experiment
Super-hard

ABSTRACT

High-entropy ceramic coatings have some unique physical and mechanical properties, such as high hardness, good corrosion resistance and excellent thermal stability. However, since they can contain five or more metal elements, their composition is quite complex. Combined with machine learning and high-throughput experimental methods, ultra-hard high-entropy ceramic coatings were screened in a short period of time. The hardness of coatings is predicted using a random forest algorithm based on its composition and processing parameters. The uncertainty of machine learning prediction is further reduced by active learning. After three iterations, a new high-entropy ceramic coating (AlCrNbTaTi)N with a hardness of 40.1 GPa has been successfully prepared, which is 9% higher than the optimal hardness of the original quinary system. This paper demonstrates that machine learning combined with high-throughput experimental methods can effectively accelerate design and composition optimization of multicomponent materials.

1. Introduction

Due to the high hardness, excellent oxidation and wear resistance, transition metal nitrides (TMNs) coatings are widely used with structural or functional materials to protect them from wear damage [1-4]. Among TMNs, TiN and CrN are common protective coatings due to their exceptional mechanical properties [5,6]. However, the rapid oxidation of TiN at 550 °C limits its industrial applications. The addition of Al into either TiN or CrN increases the oxidation resistance up to 950 °C [7]. Thus, alloying is an effective method to improve the properties of coatings. However, most studies are limited to ternary or quaternary systems (without nitrogen compounds).

Recently, numerous high-entropy alloy nitride (HEAN) coatings have been investigated [8-10]. Due to high-entropy and slow diffusion effects, HEAN coatings easily form a single-phase structure, which has been found to exhibit several unique properties, such as good thermal stability, excellent mechanical properties and corrosion resistance [11-14]. Thus, HEAN is a potential candidate material for the next generation of protective hard coatings [15]. HEAN coatings are generally made up of five or more metal elements, and the number of possible components is much higher than in traditional coatings. Due to the complexity of HEAN coatings, traditional "trial and error" experiments are expensive and time-consuming.

In recent years, machine learning (ML) has been applied in the field of material science, providing solutions to complex problems [16,17]. With the assistance of appropriate descriptors, ML has been successfully applied for the design of new materials, such as bulk metallic glasses [18], light-emitting diodes [19], shape memory alloys [20] and inorganic-organic hybrid materials [21]. Moreover, by establishing the relationship between material composition and performance, ML can realize the efficient and reasonable design of material composition. Wang et al. established a machine learning design system for predicting ultimate tensile strength and conductivity based on copper alloy composition and realized its reverse design [22]. In the field of high-entropy materials, Wen et al. developed a material design strategy for finding high-entropy alloys with high hardness in the

* Corresponding author. Beijing Advanced Innovation Center for Materials Genome Engineering, University of Science and Technology Beijing, Beijing, 100083, China
** Corresponding author. Beijing Advanced Innovation Center for Materials Genome Engineering, University of Science and Technology Beijing, Beijing, 100083, China.
E-mail addresses: taoguo@ustb.edu.cn (T. Guo), pangxl@mater.ustb.edu.cn (X. Pang).

https://doi.org/10.1016/j.ceramint.2022.07.145
Received 7 May 2022; Received in revised form 6 July 2022; Accepted 9 July 2022
Available online 30 July 2022

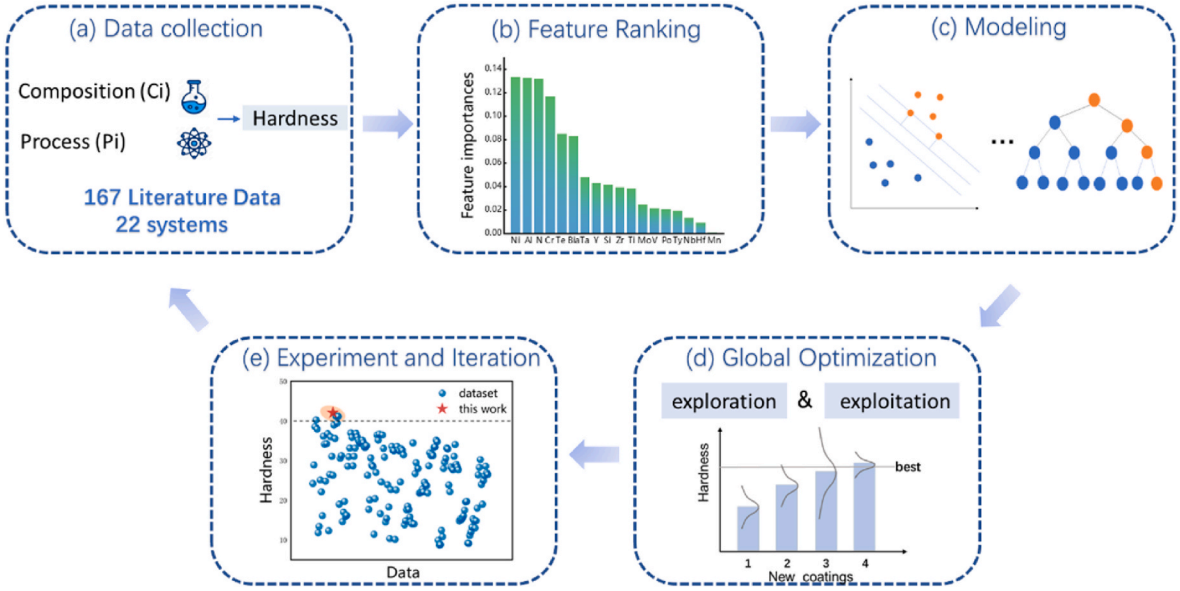

Fig. 1. Schematic design of a high-entropy ceramic coating with high hardness. (a) Data collection (b) The input features are sorted by random forest. (c) Modeling insert space Feature importance exploration and applications. (d) Use active learning to balance development and exploration. (e) Experimental verification and iterative methods are used to predict and prepare new coatings.

Al–Co–Cr–Cu–Fe–Ni system [23]. Kaufmann et al. used thermodynamic and compositional attributes to predict the entropy-forming ability (EFA) of disordered metal carbides [24]. These examples prove that machine learning is a useful tool for the discovery of multicomponent materials. However, most of these studies focus on bulk materials, with only a few studies of coatings. Banko et al. used generative machine learning methods to predict SEM surface images of thin films, which can be applied for the optimization of chemical composition and processing parameters to achieve a desired microstructure [25]. In addition to machine learning, using active learning to select the next experiment can accelerate the discovery of new materials with excellent performance, such as the discovery of high-strength magnesium alloys and the search for shape memory alloys with low transition temperature [26, 27]. Furthermore, high-throughput methods are also frequently used in the preparation of coatings to speed up the discovery of new materials [28]. Song et al. presented a high-throughput strategy where 97 independent nanocrystalline alloy samples with homogeneous element distribution can be prepared simultaneously through multi-station rotary sample stage [29].

In this study, a material design strategy combining machine learning and high-throughput experiments is proposed to rapidly screen ultra-hard high-entropy ceramic coatings. The composition and process parameters of the coating are used to predict the hardness. The coating hardness predicted by this method is 9% higher than in the quinary system from the original training dataset. These coatings were successfully synthesized through high-throughput experiments. Machine learning combined with high-throughput experimental methods can effectively accelerate the composition design of multi-component materials.

2. Materials and methods

2.1. Design strategy

The whole material design strategy schematics based on machine learning is shown in Fig. 1. The data collection and processing steps are the basis of machine learning, and the input variables are composed of the coating composition and the preparation process. Then the variables are sorted and analyzed to determine the relationship between the input variables and the impact on output variables. The prediction accuracy of different models is compared through 10-fold cross-validation, and the RF model is finally selected. Because of the uncertainty of ML prediction, the EGO algorithm is used to identify the super-hard coatings from the search space. Finally, coatings were prepared by high-throughput experiments, and newly obtained experimental data were added to the training data for the next iteration.

2.2. Machine learning models

Six types of common machine learning models were applied, including linear regression (Lin), linear kernel support vector regression (SVR.l), polynomial kernel support vector regression (SVR.p), radial kernel support vector regression (SVR.r), random forest (RF) and gradient boosting regression (GBR) models. All ML models were established and trained by the scikit-learn library in the Python environment. The original data was divided into a training set and a testing set, and the training set is taken from 50% to 90% of the original dataset.

Pearson correlation coefficient, p, was used to evaluate the correlation of features:

$$p = \frac{\sum_{i=1}^{n}(x_i - \bar{x})(y_i - \bar{y})}{\sqrt{\sum_{i=1}^{n}(x_i - \bar{x})^2}\sqrt{(y_i - \bar{y})^2}} \quad (1)$$

here, x_i and y_i are features for comparison. The p value varies from 0 to 1. The higher the value of p, the greater the correlation between the two features.

In addition, determinant coefficients (R^2) and root mean square error (RMSE) were used to evaluate the predictive performance of the model through 10-fold cross-validation [30]:

$$R^2 = 1 - \frac{\sum_{i=1}^{n}(y_i - \hat{y}_i)^2}{\sum_{i=1}^{n}(y_i - \bar{y}_i)^2} \quad (2)$$

$$RMSE = \sqrt{\frac{1}{n}\sum_{i=1}^{n}(y_i - \hat{y}_i)^2} \quad (3)$$

here, y_i, $\hat{y}_i$ and $\bar{y}_i$ represent the measured value, the predicted value, and the average value of the hardness, respectively.

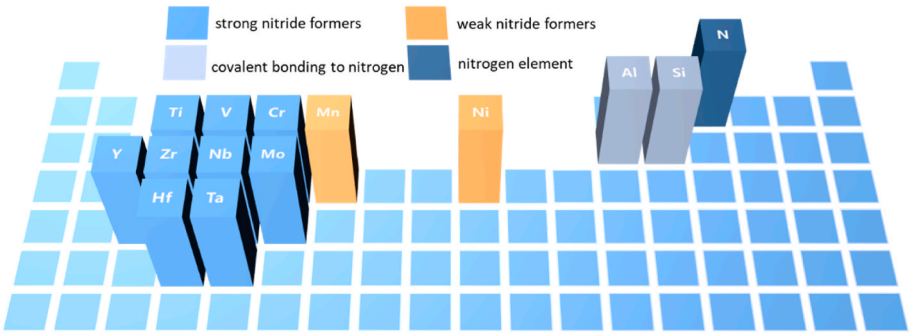

Fig. 2. Elemental components of high-entropy nitride coatings, including strong nitride formers, weak nitride formers, and p-elements that form a covalent bond with N.

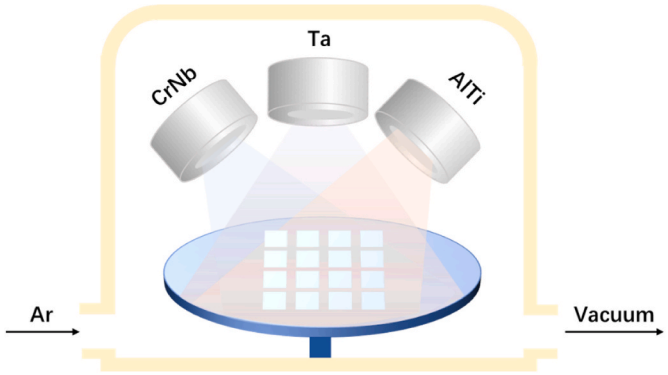

Fig. 3. Schematic diagram of magnetron co-sputtering process.

2.3. Search space

The composition space of the HEAN coatings corresponds to a large search space, since it is composed of different systems. As shown in Fig. 2, the elements forming the nitride coating can be divided into strong and weak nitride-forming elements. Strong nitride-forming elements are composed of IV to VI groups of metals, including aluminum and silicon. Weak nitride-forming elements such as manganese and nickel will degrade the mechanical properties of the coating. A total of 252 high-entropy ceramic systems can be formed by selecting 5 metals from 10 strong nitriding-forming elements. Considering the preparation of the coating, the small accuracy is not appropriate, so the step size of composition change is 1%. The variation range of each element composition is from the minimum value in the dataset to 35%, and the sum of all elements is 100%.

2.4. Active learning

As mentioned in the above section, the search space of high-entropy ceramic coatings is very large, and the training data only accounts for a small part of it. There is a great uncertainty in relying only on the ML model to find the best coating system. Therefore, a utility function is introduced to calculate the maximum expected improvement (EI) of the target attribute to select the next experiment [31-33]. The EI can balance exploration (to improve prediction models) and application (to find the best forecast). The utility function is defined as $EI(\mu,\sigma) = [\varphi(z) + z\Phi(z)]$, where μandσare the average and standard deviation of the predicted hardness of the new material selected using the current alternative model, and $z = (\mu - \mu^*)/\sigma$, where μ^* is the maximum hardness in the current training data. In order to estimate the uncertainty of prediction, bootstrap sampling is performed. First, the training set is generated by bootstrap sampling, on which the RF model is trained, and then the hardness of each coating is predicted in the search space. This step is repeat 1,000 times to search 1,000 hardness values for each coating. Thereafter, the average predicted value and standard deviation of target performance corresponding to each coating component are namedμandσ. Materials with the highest EI were selected for preparation.

2.5. Experimental procedure

The coatings were deposited on Si (100) substrates (10 mm × 10 mm × 0.4 mm) using the JCP 500 magnetron sputtering system equipped with three targets. The schematic diagram of magnetron sputtering system is shown in Fig. 3. Magnetron co-sputtering is a common method in high-throughput preparation. By adjusting the height and the angle of the targets, a large number of thin film samples can be prepared in one sputtering process. AlTi, CrNb, and Ta targets were used for high-throughput coatings preparation, and 16 samples with gradient composition distribution could be prepared at one time. The power of AlTi, CrNb and Ta targets are 80W, 100W and 80W, respectively. The base pressure was 1.8×10^{-3} Pa and then substrates were cleaned by Ar^+ ions etching for 10 min. The reactive gas flow was 20 sccm Ar and 8 sccm N_2, and the deposition pressure was kept at 0.2 Pa. All depositions were implemented at a substrate temperature of 400 °C and a bias voltage of −100 V for 3 h. The in-situ nanomechanical testing system G200 of Keysight technologies company of China was used to measure the hardness under a 5 mN load. Each coating sample was measured three times to calculate the average hardness value. The phase structure of the coating was determined by grazing incidence X-ray diffraction (GIXRD, Bruker D8 Advance, Germany). The microstructure and element distribution of the coating were analyzed by scanning electron microscope (SEM, ZeissEVO-18, ZEISS, Germany) equipped with an energy dispersive spectrometer (EDS). The composition of each coating sample is measured at different locations to ensure uniformity of the sample.

3. Results and discussion

3.1. Data collection

Data were collected from the literature on high-entropy nitride coatings published since 2004. The hardness data of 22 high-entropy nitride systems were collected, including the chemical composition of the coating and three typical process conditions (substrate temperature, sputtering power and bias). In order to reduce the effects of processing on the final performance, the training data from the literature were from the coatings with good surface morphology prepared by magnetron sputtering on Si (100) substrates. The training data contained 167 samples, including 123 quinary coatings and 44 six-component coatings (the number of elements did not include nitrogen compounds). The distribution of each element in the data set is shown in Fig. 4(a). The data conform to the normal distribution, in which the content of N varies

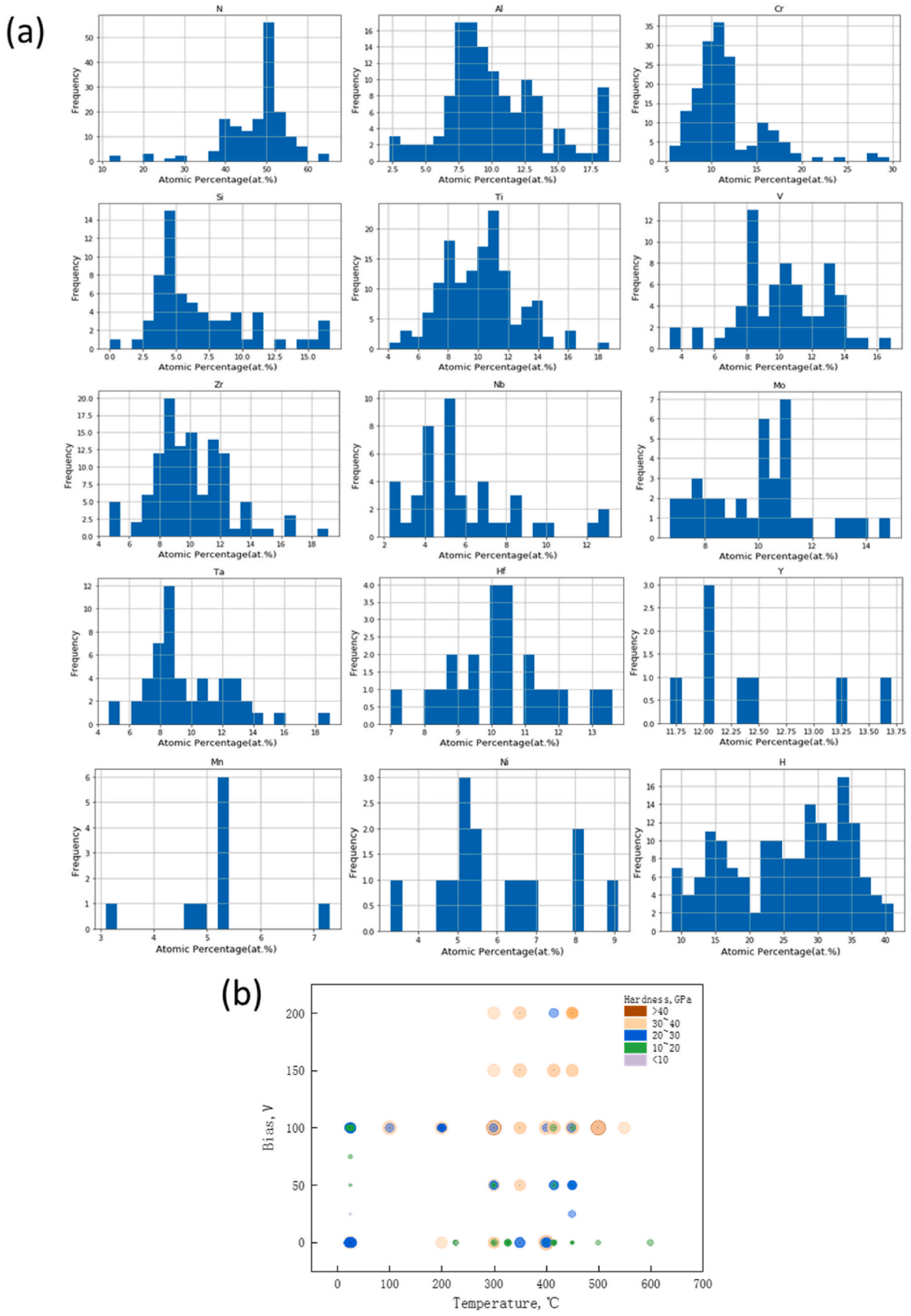

Fig. 4. Frequency distribution histogram of (a) element composition and hardness in the data set. (b) Influence of temperature and bias on hardness.

Table 1
List of coatings and research papers from which the experimental data were mined.

System	Year	System	Year
(AlCrTaTiZr)N [49]	2006	(AlCrMoNiTi)N [50]	2013
(AlCrSiTiV)N [5]	2007	(AlCrMoZrTi)N [50]	2013
(AlCrTaTiZr)N [51]	2007	(AlCrMnMoNiZr)N [35]	2013
(AlCrMoSiTi)N [52]	2008	(AlCrMnMoNiZr)N [53]	2013
(AlCrTaTiZr)N [54]	2008	(TiVCrZrHf)N [55]	2014
(AlCrNbSiTiV)N [56]	2009	(AlCrTaTiZrSi)N [57]	2014
(TiVCrZrY)N [58]	2010	(CrTaTiVZr)N [59]	2015
(AlCrTaTiZr)N [60]	2010	(CrTaTiVZr)N [61]	2015
(AlCrMoTaTiZr)N [2]	2011	(AlCrNbSiTiV)N [62]	2018
(AlCrTaTiZrSi)N [63]	2011	(AlCrTiZrNb)N [64]	2018
(TiVCrZrHf)N [65]	2011	(AlCrNbSiTiV)N [62]	2018
(AlCrNbSiTi)N [66]	2012	(CrTaTiVZr)N [67]	2020
(AlCrSiTiZr)N [68]	2012	(AlCrNbSiV)N [69]	2020
(TiVCrZrHf)N [47]	2012	(AlCrSiNbZr)N [70]	2020
(AlCrNbSiTi)N [71]	2013	(AlCrTiZrHf)N [72]	2020
(AlCrMoTaTi)N [8]	2013	(AlCrTiZrV)N [73]	2020
(TiVCrZrHf)N [74]	2013	(AlCrTiZrMoSi)N [9]	2021
(TiVCrZrY)N [75]	2013		

from 11.8% to 65.3%, and the content of metal elements varies from 2% to 30%. The amount of the first ten strong nitride-forming elements such as Al and Cr is large, ranging from dozens to more than 100. However, for Y, Mn, and Ni, the data amount is in single digits. The distribution range of hardness is from 8.6 to 41.1 GPa. Fig. 4(b) shows the correlation between hardness and processing parameters. Different colors and sizes represent different values of hardness. As seen in the figure, the coatings deposited at 300–400 °C and 100 V bias voltage usually have high hardness, which also guides the processing conditions for subsequent experiments. Table 1 lists all the literature data collected in the database.

3.2. Feature importance ranking

The Pearson correlation map is shown Fig. 5, along with the relative importance of the analyzed features. Te, Po, and Bia are abbreviations of temperature, power, and bias voltage, respectively. In Fig. 5(a), each block in the matrix represents the correlation between two different input variables, and no features with strong correlation were identified (i.e., Pearson correlation coefficient $\geq$0.9) [34]. The correlation coefficient between Mn and Ni is 0.7, which is the highest correlation. The reason for this phenomenon is that in the HEAN coatings system formed by non-nitride elements, Mn and Ni usually appear in pairs [35]. This is also captured by the correlation analysis. Fig. 5(b) displays the correlation between input characteristics and hardness using the RF method. The Bia is the most important variable, followed by the variable Al,Cr,N. However, whether the input variables have a negative or positive impact on relative importance cannot be determined. This effect is subsequently explained by shapely additive interpretation (SHAP), as shown in Fig. 6. Nitrogen content is an important factor affecting the hardness of the coating. When the nitrogen content is too low, the coating is amorphous, resulting in low hardness below 20 GPa. When the nitrogen content is sufficient, the coating can form a single solid solution structure, and the hardness of the coating can reach more than 30 GPa [36]. Adding Al, Cr, and Ta, which are strong nitride forming elements, to the coating can improve the hardness. In the process parameters, temperature and bias voltage have a great influence on the hardness, but the power has little effect. The increase of substrate temperature improves the adsorption capacity and surface mobility of atoms. Therefore, grains grow easily, and the lattice constant shows a downward trend, which eventually leads to the change of coating hardness [37,38]. With the increase of bias voltage, the energy of ions bombarding the target increases, which is conducive to the diffusion of target atoms and the ability to participate in chemical reactions. The density and film-forming properties of the coating are also improved, and finally, the hardness is improved [39, 40].

Most machine learning models are black boxes, which makes it necessary to explain this black box model for the development of new material design principles. Therefore, SHAP was used to explain the model [41]. SHAP can identify whether the contribution of input variables to each prediction is positive or negative. Fig. 6 displays the SHAP summary plot, in which each point is a sample. The change from red to blue represents the value of SHAP from high to low [42]. A positive value indicates that the variable is beneficial to the output, and a negative value indicates that the variable is harmful to the output. As seen in Fig. 6, Bia, N, and Ni are the three most important input variables affecting hardness. The effect of Bia and N on coating hardness has been discussed above. With the increase of Ni content, the SHAP value and hardness decreased. Ni is a weak nitride-forming element, which tends to form an alternative solid solution during coating deposition, and the solid solution strengthening effect is not as good as MeN_x. Therefore, coatings composed of weak nitride-forming elements usually have poor mechanical properties [35]. The high values of Al , Ta and the low values of Cr have a positive impact on the ML model, thus guiding the addition amount of metal elements. The addition of Y and Si will also reduce the hardness of the coating.

SHAP determined that N is the second important variable, while the importance ranking of RF considers Al as the second important variable. This is due to the fundamental differences in the way input variables are evaluated. Nevertheless, the first six variables determined by the RF algorithm and SHAP are the same.

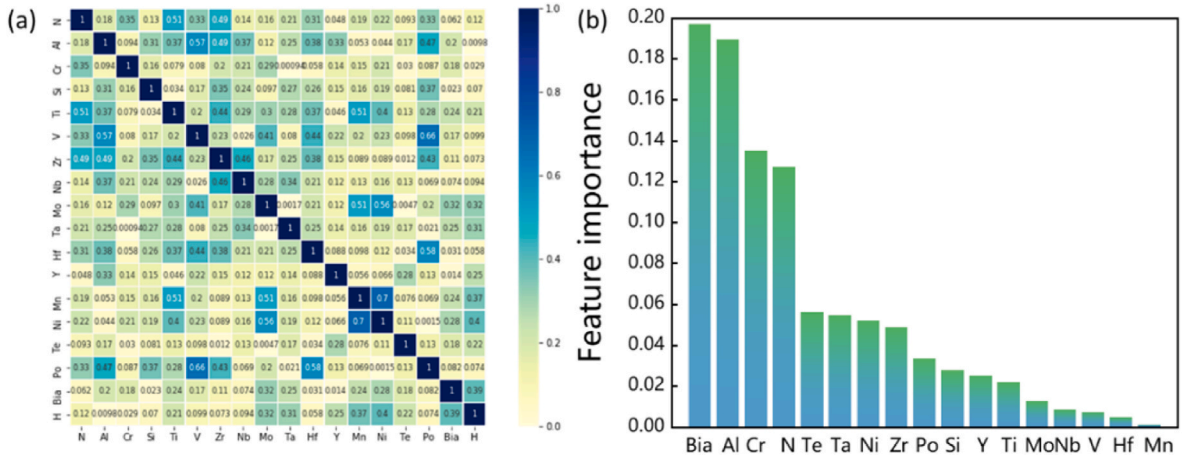

Fig. 5. The importance and correlation diagram of features. (a) Pearson correlation map of features and (b) Importance ranking of features.

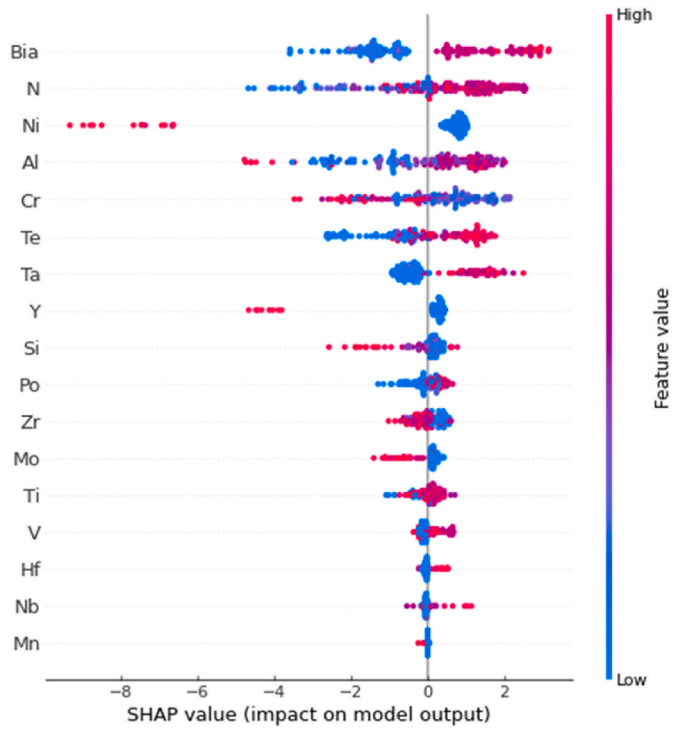

Fig. 6. Global interpretation using SHAP.

3.3. Comparison of machine learning models

The errors of machine learning models with different test set partitioning ratios are shown in Fig. 7(a). As the proportion of training set increases, the error of the model decreases. Finally, 80% of the training sets were selected. Fig. 7(b) shows the RMSE results of all models, in which the test set errors of SVR.r, RF and GBR models are significantly lower than those of the other three models. The test set error of RF and GBR model is almost the same, but the error of GBR training set is obviously lower than RF.There may be an overfitting phenomenon in GBR. RF is an integrated regression model composed of multiple decision trees. The RF model will randomly sample the original data set to form n different sample data sets, then build n different decision tree models according to these data sets, and finally, obtain the final results according to the average value (for regression model) or voting (for classification model) of these decision tree models. The advantage is that the prediction results will be more accurate. SVR can effectively deal with nonlinear problems by mapping input samples from low-dimensional space to high-dimensional space through kernel function, which is suitable for small-scale and high-dimensional data sets. The types of kernel functions that can be used in the SVR model include linear kernel function, polynomial kernel function, radial basis function (RBF) kernel function, and S-shaped kernel function. Among them, the RBF kernel is recommended and most commonly used. In this paper, the prediction results of SVR.r and RF were further compared, and the RF model is selected for subsequent prediction.

The hardness prediction of the RF model is depicted in Fig. 7(c). The data points are distributed around the diagonal, which indicates that the ML model has good performance [43]. The predicted RMSE and R^2 values are 2.3 GPa and 0.92, respectively. The relative percentage error of the predicted value is calculated. It is found that the ML model has a high accuracy, in which more than 82% of the coating hardness error is less than ±15%, and more than 74% of the coating hardness error is less than ±10%. In general, the RF model shows good statistical and predictive ability, so the RF model is adopted in this study.

3.4. Experiments and iterations

An iterative process was used to validate the potential of machine

Table 2
Composition and properties of three new coatings.

Coatings No.	Elemental content, at.%						Hardness, GPa	
	N	AI	Cr	Nb	Ta	Ti	predicted	experimental
1	49	15	12	2	19	4	33.8	37.9
2	50	16	4	1	25	4	34.9	38.5
3	48	16	15	4	8	9	35.7	40.1

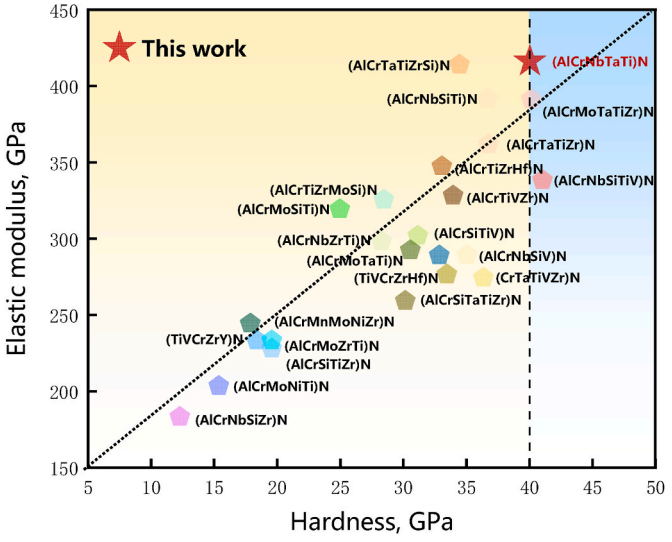

Fig. 8. Comparison of mechanical properties of high-entropy ceramic coatings.

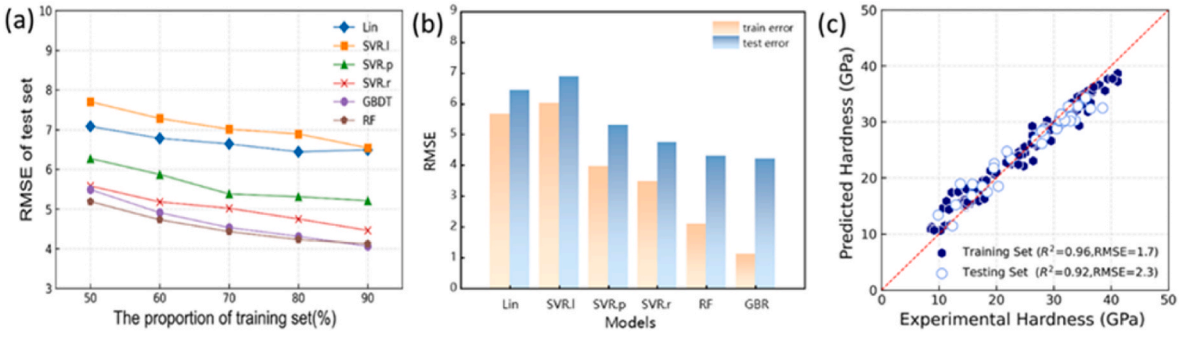

Fig. 7. Evaluation and selection of models. (a) Error of machine learning model with different partition scale of test set. (b) Train error and test error of different machine learning models. (c) Fitting results of random forest model.

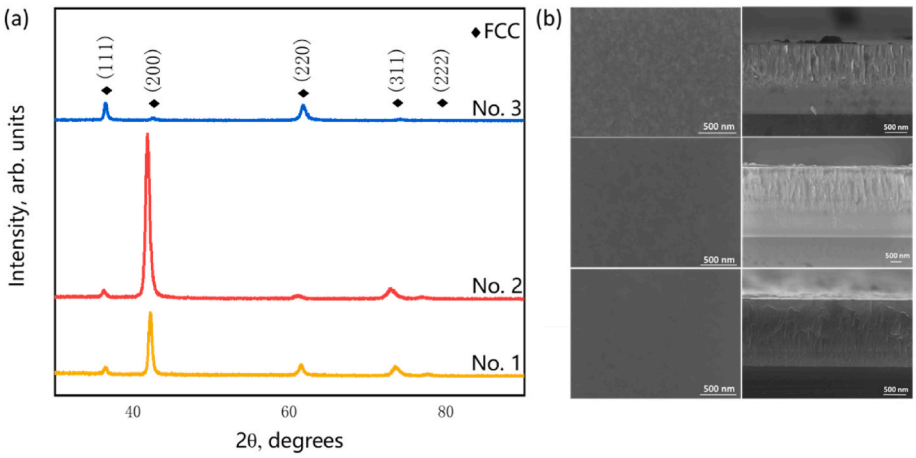

Fig. 9. (a) XRD patterns and (b) SEM images of coating top surface and cross-section.

learning in discovering high-performance HEAN coatings. The hardness of 252 systems was predicted in the search space, and the new system with the highest hardness (AlCrNbTaTi)N was selected for subsequent synthesis. Considering that the composition of the sample prepared by magnetron sputtering is difficult to control, the coating is sputtered by the high-throughput preparation method [39]. By adjusting the sputtering power of the target gun, 16(AlCrNbTaTi)N coating samples can be prepared in one run. Coating hardness can be measured by nano-indentation. The coatings whose relative error between the predicted hardness and the experimental hardness is less than 15% are considered to be added to the original data for the next iteration. In the third iteration, coating with a hardness of 40.1 GPa was found. The predicted and experimental values of the coating during each iteration are listed in Table 2, and the hardness ranges from 37.9 GPa to 40.1 GPa. The predicted hardness is lower than the measured value, and the average prediction error is 11.5%, which indicates that the ML model of composition and process parameters is used to adequately predict the performance of the new coating. It is worth noting that in these three iterations, the predicted values are usually lower than the experimental values, indicating that the generalization ability of the model is limited due to the lack of high-quality data [44].

The hardness of the coatings with the best performance was compared with the coatings in the data set, as shown in Fig. 8. The red five-pointed star is the measured hardness of the coating prepared in this work. The pentagon represents the sample with the highest hardness of each system in the data set, and the system is marked in the figure. This value is 9% higher than the maximum hardness (36.9 GPa) of the quinary system in the original data [45], and only 1 GPa lower than the maximum hardness value of the six-component system, which can be considered as the measurement error [46].

The phase and microstructure of the three coatings were studied. In Fig. 9(a) XRD results show that the three coatings form high-entropy ceramics with a single FCC solid solution phase structure. Fig. 9(b) show the SEM morphology of the three coatings. The coating exhibits a very smooth surface without any obvious features. From the cross-sectional morphology of the coating, it can be observed that two different layers are separated by the boundary. The underlayer shows an amorphous structure, whereas the upper layer had a nano grain structure. In the present study, the formation of the amorphous phase is caused by the tremendous compressive stress during deposition and the serious lattice distortion of multiple principal components. With the continuous deposition, the structures of Cr, Nb, Ta, and Ti binary nitrides are FCC structure, which can be attributed to the high mixing entropy effect. This structure has also been reported in other papers [47, 48]. Good surface and cross-section morphology is also one of the reasons for the high hardness of the coating.

4. Conclusions

In this study, a method combining machine learning and high-throughput experiments is proposed to predict and prepare a new super-hard high-entropy ceramic coating system, which is the hardest quinary system reported so far. The data were collected on the composition and process parameters of 22 high-entropy nitride coating systems. Based on the RF algorithm and SHAP, the relationship between hardness and input characteristics is analyzed. The key factors affecting the hardness of the coating are Bia, Al, Cr, and N. After comparing several common ML algorithms, an RF algorithm was selected, and active learning was introduced to further reduce the prediction error. Through three iterations, a new high-entropy nitride coating (AlCrNbTaTi)N was found. Its hardness was 40.1 GPa, 9% higher than the quinary system in the original data set and only 1 GPa lower than the six-component system. Finally, the phase identification and microstructure characterization of the coating were carried out, and it was found that the coating formed a single FCC structure. These results show that the ML-based method has great potential in manufacturing super-hard high-entropy ceramic coatings. The design strategy can be used to optimize the corrosion resistance and wear resistance of the coatings.

Declaration of competing interest

The authors declare that they have no known competing financial interests or personal relationships that could have appeared to influence the work reported in this paper.

Acknowledgments

This work was supported by the National Natural Science Foundation of China (Nos. 51922002, U21A2044), Fundamental Research Funds for the Central Universities (FRF-TP-17-19-003C1Z), and the Science Center for Gas Turbine Project (Grant No. P2021-A-IV-002-001).

References

[1] V. Attari, A. Cruzado, R. Arroyave, Exploration of the microstructure space in TiAlZrN ultra-hard nanostructured coatings, Acta Mater. 174 (2019) 459–476.
[2] K.-H. Cheng, C.-H. Lai, S.-J. Lin, J.-W. Yeh, Structural and mechanical properties of multi-element (AlCrMoTaTiZr)Nx coatings by reactive magnetron sputtering, Thin Solid Films 519 (10) (2011) 3185–3190.
[3] M. Mikula, D. Plasienka, D.G. Sangiovanni, M. Sahul, T. Roch, M. Truchly, M. Gregor, L. Caplovic, A. Plecenik, P. Kus, Toughness enhancement in highly NbN-alloyed Ti-Al-N hard coatings, Acta Mater. 121 (2016) 59–67.
[4] G. Abadias, L.E. Koutsokeras, S.N. Dub, G.N. Tolmachova, A. Debelle, T. Sauvage, P. Villechaise, Reactive magnetron cosputtering of hard and conductive ternary nitride thin films: Ti–Zr–N and Ti–Ta–N, J. Vac. Sci. Technol.: Vacuum, Surfaces, and Films 28 (4) (2010) 541–551.

[5] C.H. Lin, J.G. Duh, J.W. Yeh, Multi-component nitride coatings derived from Ti–Al–Cr–Si–V target in RF magnetron sputter, Surf. Coating. Technol. 201 (14) (2007) 6304–6308.
[6] P. Panjan, B. Navinsek, A. Cvelbar, A. Zalar, J. Vlcek, High-temperature oxidation of TiN/CrN multilayers reactively sputtered at low temperatures, Surf. Coating. Technol. 98 (1-3) (1998) 1497–1502.
[7] S. PalDey, S.C. Deevi, Single layer and multilayer wear resistant coatings of (Ti,Al)N: a review, Mater. Sci. Eng., A 342 (1-2) (2003) 58–79.
[8] D.C. Tsai, Z.C. Chang, B.H. Kuo, M.H. Shiao, S.Y. Chang, F.S. Shieu, Structural morphology and characterization of (AlCrMoTaTi)N coating deposited via magnetron sputtering, Appl. Surf. Sci. 282 (2013) 789–797.
[9] W. Yu, W. Li, P. Liu, K. Zhang, F. Ma, X. Chen, R. Feng, P.K. Liaw, Silicon-content-dependent microstructures and mechanical behavior of (AlCrTiZrMo)-Six-N high-entropy alloy nitride films, Mater. Des. (2021) 203.
[10] W.L. Lo, S.Y. Hsu, Y.C. Lin, S.Y. Tsai, Y.T. Lai, J.G. Duh, Improvement of high entropy alloy nitride coatings (AlCrNbSiTiMo)N on mechanical and high temperature tribological properties by tuning substrate bias, Surf. Coating. Technol. (2020) 401.
[11] J.W. Yeh, S.K. Chen, S.J. Lin, J.Y. Gan, T.S. Chin, T.T. Shun, C.H. Tsau, S.Y. Chang, Nanostructured high-entropy alloys with multiple principal elements: novel alloy design concepts and outcomes, Adv. Eng. Mater. 6 (5) (2004) 299–303.
[12] P.K. Huang, J.W. Yeh, T.T. Shun, S.K. Chen, Multi-principal-element alloys with improved oxidation and wear resistance for thermal spray coating, Adv. Eng. Mater. 6 (1-2) (2004) 74–78.
[13] C.Y. Hsu, J.W. Yeh, S.K. Chen, T.T. Shun, Wear resistance and high-temperature compression strength of Fcc CuCoNiCrAl0.5Fe alloy with boron addition, Metall. Mater. Trans. A 35a (5) (2004) 1465–1469.
[14] C.J. Tong, Y.L. Chen, S.K. Chen, J.W. Yeh, T.T. Shun, C.H. Tsau, S.J. Lin, S. Y. Chang, Microstructure characterization of AlxCoCrCuFeNi high-entropy alloy system with multi principal elements, Metall. Mater. Trans. A 36a (4) (2005) 881–893.
[15] T.-C. Huang, S.-Y. Hsu, Y.-T. Lai, S.-Y. Tsai, J.-G. Duh, Effect of NiTi metallic layer thickness on scratch resistance and wear behavior of high entropy alloy (CrAlNbSiV) nitride coating, Surf. Coating. Technol. (2021) 425.
[16] K.T. Butler, D.W. Davies, H. Cartwright, O. Isayev, A. Walsh, Machine learning for molecular and materials science, Nature 559 (7715) (2018) 547–555.
[17] L. Himanen, A. Geurts, A.S. Foster, P. Rinke, Data-driven materials science: status, challenges, and perspectives, Adv. Sci. 6 (21) (2019).
[18] F. Ren, L. Ward, T. Williams, K.J. Laws, C. Wolverton, J. Hattrick-Simpers, A. Mehta, Accelerated discovery of metallic glasses through iteration of machine learning and high-throughput experiments, Sci. Adv. 4 (4) (2018).
[19] B. Rouet-Leduc, K. Barros, T. Lookman, C.J. Humphreys, Optimisation of GaN LEDs and the reduction of efficiency droop using active machine learning, Sci. Rep. 6 (2016), 24862.
[20] D. Xue, P.V. Balachandran, J. Hogden, J. Theiler, D. Xue, T. Lookman, Accelerated search for materials with targeted properties by adaptive design, Nat. Commun. 7 (2016), 11241.
[21] S. Lu, Q. Zhou, Y. Ouyang, Y. Guo, Q. Li, J. Wang, Accelerated discovery of stable lead-free hybrid organic-inorganic perovskites via machine learning, Nat. Commun. 9 (1) (2018) 3405.
[22] C. Wang, H. Fu, L. Jiang, D. Xue, J. Xie, A property-oriented design strategy for high performance copper alloys via machine learning, npj Comput. Mater. 5 (1) (2019).
[23] C. Wen, Y. Zhang, C. Wang, D. Xue, Y. Bai, S. Antonov, L. Dai, T. Lookman, Y. Su, Machine learning assisted design of high entropy alloys with desired property, Acta Mater. 170 (2019) 109–117.
[24] K. Kaufmann, D. Maryanovsky, W.M. Mellor, C.Y. Zhu, A.S. Rosengarten, T. J. Harrington, C. Oses, C. Toher, S. Curtarolo, K.S. Vecchio, Discovery of high-entropy ceramics via machine learning, Npj Comput. Mater. 6 (1) (2020).
[25] L. Banko, Y. Lysogorskiy, D. Grochla, D. Naujoks, R. Drautz, A. Ludwig, Predicting structure zone diagrams for thin film synthesis by generative machine learning, Commun. Mater. 1 (1) (2020).
[26] Y.W. Liu, L.Y. Wang, H.A. Zhang, G.M. Zhu, J. Wang, Y.H. Zhang, X.Q. Zeng, Accelerated development of high-strength magnesium alloys by machine learning, Metall. Mater. Trans. A 52 (3) (2021) 943–954.
[27] D.Z. Xue, D.Q. Xue, R.H. Yuan, Y.M. Zhou, P.V. Balachandran, X.D. Ding, J. Sun, T. Lookman, An informatics approach to transformation temperatures of NiTi-based shape memory alloys, Acta Mater. 125 (2017) 532–541.
[28] A. Ludwig, Discovery of new materials using combinatorial synthesis and high-throughput characterization of thin-film materials libraries combined with computational methods, Npj Comput. Mater. 5 (2019).
[29] Y. Song, L. Yan, X. Pang, Y. Su, L. Qiao, K. Gao, High-throughput preparation and electrochemical screening of nanocrystalline Fe-Cr-Ni material libraries with homogeneous element distribution, Corrosion Sci. (2022) 196.
[30] H. Wang, C. Ji, C. Shi, Y. Ge, H. Meng, J. Yang, K. Chang, S. Wang, Comparison and evaluation of advanced machine learning methods for performance and emissions prediction of a gasoline Wankel rotary engine, Energy (2022) 248.
[31] D.Z. Xue, P.V. Balachandran, J. Hogden, J. Theiler, D.Q. Xue, T. Lookman, Accelerated search for materials with targeted properties by adaptive design, Nat. Commun. 7 (2016).
[32] T. Lookman, P.V. Balachandran, D.Z. Xue, J. Hogden, J. Theiler, Statistical inference and adaptive design for materials discovery, Curr. Opin. Solid State Mater. Sci. 21 (3) (2017) 121–128.
[33] R.H. Yuan, Z. Liu, P.V. Balachandran, D.Q. Xue, Y.M. Zhou, X.D. Ding, J. Sun, D. Z. Xue, T. Lookman, Accelerated discovery of large electrostrains in BaTiO3-based piezoelectrics using active learning, Adv. Mater. 30 (7) (2018).
[34] H.H. Xu, Y. Deng, Dependent evidence combination based on shearman coefficient and Pearson coefficient, IEEE Access 6 (2018) 11634–11640.
[35] B. Ren, Z. Shen, Z. Liu, Structure and mechanical properties of multi-element (AlCrMnMoNiZr)Nx coatings by reactive magnetron sputtering, J. Alloys Compd. 560 (2013) 171–176.
[36] E. Lewin, Multi-component and high-entropy nitride coatings-A promising field in need of a novel approach, J. Appl. Phys. 127 (16) (2020).
[37] K. von Fieandt, E.M. Paschalidou, A. Srinath, P. Soucek, L. Riekehr, L. Nyholm, E. Lewin, Multi-component (Al,Cr,Nb,Y,Zr)N thin films by reactive magnetron sputter deposition for increased hardness and corrosion resistance, Thin Solid Films (2020) 693.
[38] Y.C. Lin, S.Y. Hsu, R.W. Song, W.L. Lo, Y.T. Lai, S.Y. Tsai, J.G. Duh, Improving the hardness of high entropy nitride (Cr0.35Al0.25Nb0.12Si0.08V0.20)N coatings via tuning substrate temperature and bias for anti-wear applications, Surf. Coating. Technol. (2020) 403.
[39] X.H. Yan, J.S. Li, W.R. Zhang, Y. Zhang, A brief review of high-entropy films, Mater. Chem. Phys. 210 (2018) 12–19.
[40] J.J. Wang, S.Y. Chang, F.Y. Ouyang, Effect of substrate bias on the microstructure and properties of (AlCrSiNbZr) Nx high entropy nitride thin film, Surf. Coating. Technol. (2020) 393.
[41] S.M. Lundberg, S.I. Lee, A unified approach to interpreting model predictions, Adv. Neural Inf. Process. Syst. 30 (2017) 30 (Nips 2017).
[42] J. Jeon, N. Seo, S.B. Son, S.J. Lee, M. Jung, Application of machine learning algorithms and SHAP for prediction and feature analysis of tempered martensite hardness in low-alloy steels, Metals 11 (8) (2021).
[43] H.T. Zhang, H.D. Fu, X.Q. He, C.S. Wang, L. Jiang, L.Q. Chen, J.X. Xie, Dramatically enhanced combination of ultimate tensile strength and electric conductivity of alloys via machine learning screening, Acta Mater. 200 (2020) 803–810.
[44] Q.K. Zhao, H.Y. Yang, J.B. Liu, H.F. Zhou, H.T. Wang, W. Yang, Machine learning-assisted discovery of strong and conductive Cu alloys: data mining from discarded experiments and physical features, Mater. Des. (2021) 197.
[45] C.H. Lai, K.H. Cheng, S.J. Lin, J.W. Yeh, Mechanical and tribological properties of multi-element (AlCrTaTiZr)N coatings, Surf. Coating. Technol. 202 (15) (2008) 3732–3738.
[46] P.K. Huang, J.W. Yeh, Effects of substrate temperature and post-annealing on microstructure and properties of (AlCrNbSiTiV)N coatings, Thin Solid Films 518 (1) (2009) 180–184.
[47] D.C. Tsai, S.C. Liang, Z.C. Chang, T.N. Lin, M.H. Shiao, F.S. Shieu, Effects of substrate bias on structure and mechanical properties of (TiVCrZrHf)N coatings, Surf. Coating. Technol. 207 (2012) 293–299.
[48] S.C. Liang, Z.C. Chang, D.C. Tsai, Y.C. Lin, H.S. Sung, M.J. Deng, F.S. Shieu, Effects of substrate temperature on the structure and mechanical properties of (TiVCrZrHf)N coatings, Appl. Surf. Sci. 257 (17) (2011) 7709–7713.
[49] C.-H. Lai, S.-J. Lin, J.-W. Yeh, A. Davison, Effect of substrate bias on the structure and properties of multi-element (AlCrTaTiZr)N coatings, J. Phys. Appl. Phys. 39 (21) (2006) 4628–4633.
[50] B. Ren, S.Q. Yan, R.F. Zhao, Z.X. Liu, Structure and properties of (AlCrMoNiTi)Nx and (AlCrMoZrTi)Nx films by reactive RF sputtering, Surf. Coating. Technol. 235 (2013) 764–772.
[51] C.-H. Lai, M.-H. Tsai, S.-J. Lin, J.-W. Yeh, Influence of substrate temperature on structure and mechanical, properties of multi-element (AlCrTaTiZr)N coatings, Surf. Coating. Technol. 201 (16-17) (2007) 6993–6998.
[52] H.-W. Chang, P.-K. Huang, A. Davison, J.-W. Yeh, C.-H. Tsau, C.-C. Yang, Nitride films deposited from an equimolar Al–Cr–Mo–Si–Ti alloy target by reactive direct current magnetron sputtering, Thin Solid Films 516 (18) (2008) 6402–6408.
[53] B. Ren, S.J. Lv, R.F. Zhao, Z.X. Liu, S.K. Guan, Effect of sputtering parameters on (AlCrMnMoNiZr)N films, Surf. Eng. 30 (2) (2013) 152–158.
[54] C.-H. Lai, K.-H. Cheng, S.-J. Lin, J.-W. Yeh, Mechanical and tribological properties of multi-element (AlCrTaTiZr)N coatings, Surf. Coating. Technol. 202 (15) (2008) 3732–3738.
[55] D.-C. Tsai, Z.-C. Chang, B.-H. Kuo, T.-N. Lin, M.-H. Shiao, F.-S. Shieu, Interfacial reactions and characterization of (TiVCrZrHf)N thin films during thermal treatment, Surf. Coating. Technol. 240 (2014) 160–166.
[56] P.-K. Huang, J.-W. Yeh, Effects of substrate temperature and post-annealing on microstructure and properties of (AlCrNbSiTiV)N coatings, Thin Solid Films 518 (1) (2009) 180–184.
[57] S.-Y. Lin, S.-Y. Chang, C.-J. Chang, Y.-C. Huang, Nanomechanical properties and deformation behaviors of multi-component (AlCrTaTiZr)NxSiy high-entropy coatings, Entropy 16 (1) (2013) 405–417.
[58] D.-C. Tsai, Y.-L. Huang, S.-R. Lin, S.-C. Liang, F.-S. Shieu, Effect of nitrogen flow ratios on the structure and mechanical properties of (TiVCrZrY)N coatings prepared by reactive magnetron sputtering, Appl. Surf. Sci. 257 (4) (2010) 1361–1367.
[59] Z.-C. Chang, D.-C. Tsai, E.-C. Chen, Structure and characteristics of reactive magnetron sputtered (CrTaTiVZr)N coatings, Mater. Sci. Semicond. Process. 39 (2015) 30–39.
[60] S.-Y. Chang, S.-Y. Lin, Y.-C. Huang, C.-L. Wu, Mechanical properties, deformation behaviors and interface adhesion of (AlCrTaTiZr)Nx multi-component coatings, Surf. Coating. Technol. 204 (20) (2010) 3307–3314.
[61] Z.-C. Chang, D.-C. Tsai, E.-C. Chen, Effect of N2 flow on the structure and mechanical properties of (CrTaTiVZr)Nx coatings processed by reactive magnetron sputtering, J. Mater. Res. 30 (7) (2015) 924–934.
[62] C.-H. Chang, C.-B. Yang, C.-C. Sung, C.-Y. Hsu, Structure and tribological behavior of (AlCrNbSiTiV)N film deposited using direct current magnetron sputtering and high power impulse magnetron sputtering, Thin Solid Films 668 (2018) 63–68.

[63] K.-H. Cheng, C.-W. Tsai, S.-J. Lin, J.-W. Yeh, Effects of silicon content on the structure and mechanical properties of (AlCrTaTiZr)–Six–N coatings by reactive RF magnetron sputtering, J. Phys. Appl. Phys. 44 (20) (2011).
[64] C. Huang, W. Li, P. Liu, K. Zhang, X. Chen, F. Ma, K. Liu, Synthesis and mechanical properties of (AlCrTiZrNb)N high entropy alloy films grown by RF magnetron sputtering, Chinese J. Vacuum Sci. Technol. 38 (6) (2018).
[65] S.-C. Liang, D.-C. Tsai, Z.-C. Chang, H.-S. Sung, Y.-C. Lin, Y.-J. Yeh, M.-J. Deng, F.-S. Shieu, Structural and mechanical properties of multi-element (TiVCrZrHf)N coatings by reactive magnetron sputtering, Appl. Surf. Sci. 258 (1) (2011) 399–403.
[66] W.-J. Shen, M.-H. Tsai, Y.-S. Chang, J.-W. Yeh, Effects of substrate bias on the structure and mechanical properties of (Al1.5CrNb0.5Si0.5Ti)Nx coatings, Thin Solid Films 520 (19) (2012) 6183–6188.
[67] Z.-C. Chang, J.-Y. Liang, Oxidation behavior and structural transformation of (CrTaTiVZr)N coatings, Coatings 10 (4) (2020).
[68] H.-T. Hsueh, W.-J. Shen, M.-H. Tsai, J.-W. Yeh, Effect of nitrogen content and substrate bias on mechanical and corrosion properties of high-entropy films (AlCrSiTiZr)100−xNx, Surf. Coating. Technol. 206 (19-20) (2012) 4106–4112.
[69] Y.-C. Lin, S.-Y. Hsu, R.-W. Song, W.-L. Lo, Y.-T. Lai, S.-Y. Tsai, J.-G. Duh, Improving the hardness of high entropy nitride (Cr0.35Al0.25Nb0.12Si0.08V0.20)N coatings via tuning substrate temperature and bias for anti-wear applications, Surf. Coating. Technol. (2020) 403.
[70] J.-J. Wang, S.-Y. Chang, F.-Y. Ouyang, Effect of substrate bias on the microstructure and properties of (AlCrSiNbZr)Nx high entropy nitride thin film, Surf. Coating. Technol. (2020) 393.
[71] M.-H. Hsieh, M.-H. Tsai, W.-J. Shen, J.-W. Yeh, Structure and properties of two Al–Cr–Nb–Si–Ti high-entropy nitride coatings, Surf. Coating. Technol. 221 (2013) 118–123.
[72] P. Cui, W. Li, P. Liu, K. Zhang, F. Ma, X. Chen, R. Feng, P.K. Liaw, Effects of nitrogen content on microstructures and mechanical properties of (AlCrTiZrHf)N high-entropy alloy nitride films, J. Alloys Compd. (2020) 834.
[73] L. Chen, W. Li, P. Liu, K. Zhang, F. Ma, X. Chen, H. Zhou, X. Liu, Microstructure and mechanical properties of (AlCrTiZrV)Nx high-entropy alloy nitride films by reactive magnetron sputtering, Vacuum (2020) 181.
[74] D.-C. Tsai, Z.-C. Chang, L.-Y. Kuo, T.-J. Lin, T.-N. Lin, F.-S. Shieu, Solid solution coating of (TiVCrZrHf)N with unusual structural evolution, Surf. Coating. Technol. 217 (2013) 84–87.
[75] D.-C. Tsai, Z.-C. Chang, B.-H. Kuo, M.-H. Shiao, S.-Y. Chang, F.-S. Shieu, Structure and properties of (TiVCrZrY)N coatings prepared by energetic bombardment sputtering with different nitrogen flow ratios, Appl. Phys. A 115 (4) (2013) 1205–1213.